On Vortices Initiated over West Africa and Their Impact on North Atlantic Tropical Cyclones

Jean-Philippe Duvel

On vortices initiated over West Africa and their impact on North Atlantic tropical cyclones

Jean-Philippe Duvel

Laboratoire de Météorologie Dynamique, CNRS, Paris, France

Submitted to Monthly Weather Review

July 2020, revised October 2020

Author address:

Laboratoire de Météorologie Dynamique, École Normale Supérieure,

24, rue Lhomond, F75231 Paris, France

jpduvel@lmd.ipsl.fr

Abstract

Using 38 years of the ERA Interim dataset, an objective tracking approach is used to analyze the origin, characteristics and cyclogenesis efficiency (CE) of synoptic-scale vortices initiated over West Africa and the Atlantic Ocean. Many vortex tracks initiated near the coast or over the ocean result from a vertical expansion of a "primary" vortex track that was initiated earlier over West Africa. Low-level (850hPa) primary vortices are initiated mainly in July near the Hoggar mountains (5°E, 24°N), while mid-level (700 hPa) primary vortices are initiated mainly in August-September near Guinea highlands (10°W, 10°N). The CE of all these vortices is about 10% in July and 30% in August. The average CE is however smaller for low-level "Hoggar" vortices because they peak in July when the cyclogenesis potential index of the Atlantic Ocean is weak. Seasonal and interannual modulations of the cyclogenesis is related more to this index than to the *number* of vortices crossing the West African coast. Cyclogenesis is nearly equally distributed between the coast and 60°W, but the part of the cyclogenesis due to vortices initiated over West Africa decreases from 80% near the coast to about 30% at 60°W. The most probable delay between the vortex vertical expansion and cyclogenesis is 2 days, but it can be up to 10 days. This analysis also confirms previous results, such as the larger CE for vortices extending at low-levels over the continent at 10°N, or the delayed and therefore west-shifted cyclogenesis of low-level "Hoggar" vortices.

1. Introduction

Vortices initiated over West Africa are known sources of tropical storms and hurricanes over the Northern Atlantic Ocean and are mostly associated with African Easterly Waves (AEWs) (Erickson 1963, Carlson 1969, Burpee 1972, Landsea 1993, Avila et al. 2000, Hopsch et al. 2007, Russel et al. 2017). This relation between AEWs and cyclogenesis motivated several observational studies on the structure of theses waves and on their life cycle (Reed et al. 1977, Reed et al. 1988a, Duvel 1990, Thorncroft and Hodges 2001), as well as theoretical studies on their physical origin related to instabilities of the African Easterly Jet (AEJ) (e.g. Thorncroft and Hoskins 1994). Vortices associated with AEW troughs follow two main paths over West Africa that generally merge into a single path over the Atlantic Ocean (Reed et al. 1988a and 1988b, Diedhiou et al. 1999, Thorncroft and Hodges 2001, Fink and Reiner 2003, Hodges et al. 2003). The north path coincides with the low-level monsoon trough around 20°N and consists of dry low-level vortices. The south path coincides with the rainfall maximum around 10°N and consists of moist mid-level vortices associated with deep convection. Previous analysis (e.g., Reed et al. 1977, Diedhiou et al. 2002) showed that the south path draws more energy from barotropic energy conversion at the jet level, while the north path draws more energy from baroclinic energy conversion at lower levels. Vortices of the north and the south paths are often coherent features over the African Continent (Carlson 1969, Nitta and Takayabu 1985, Pytharoulis and Thorncroft 1999, Fink and Reiner 2003) (see example in Fig.1).

Some ambiguities remain on the impact of north and the south path vortices on cyclogenesis. Thorncroft and Hodges (2001), Hopsch et al. (2007) and Dieng et al. (2017) estimated that vortices from the north path generally dissipate shortly after they leave the African coast, the south path being therefore the main source of cyclogenesis. On the other

hand, Chen et al. (2008) found that among cyclogenetic AEWs, 55% are from the north path and 45% from the south path. They also noticed that cyclogenesis tend to form further west on the north path compared to the south path. With some agreement, Ross and Krishnamurti (2007) showed that both paths may lead to cyclogenesis, especially when they interact near the coast. More recently, Chen and Liu (2014) considered the influence of merging dry and wet vortices on MDR cyclogenesis. They found that among tropical cyclones (TCs) initiated from these vortices, 70% are associated with a dry vortex merging with a wet vortex.

The main objectives of this study are: (i) to clarify the origin of low- and mid-level vortices of the north and the south path and, (ii) to determine the role of these vortices in cyclogenesis depending on their origin. This study does not consider all AEWs perturbations, but persistent vortices mostly associated with the trough of developed AEWs. The initiation of a vortex (see Table 1 for the definition of different terms used in this article) can therefore be distinct from the initiation of the corresponding AEW. For example, the initiation of a persistent vortex (i.e. when it becomes identifiable in the geopotential height, see section 2.1) may result from the intensification of a relatively weak AEW initiated further east. This intensification may be due to mesoscale convective systems (MCS) (e.g., Ritchie and Holland 1997; Montgomery et al. 2006; Cecelski and Zhang 2013) and mesoscale convective vortex (MCV) (e.g. Zhang et al. 2018) developing in the trough of the wave. A persistent vortex at a given pressure level may also result from an AEW reaching a critical latitude (where the wave phase speed equals the zonal wind) favoring the creation of a “pouch” reinforcing the role of MCS in further vortex intensification and cyclogenesis (Dunkerton et al. 2009, Cecelski and Zhang 2013). To determine the origin of these vortices, a particular emphasis is put on the conjunction, or merging, of low- and mid-level vortex tracks. This does not concern only the “confluence” of low-level vortices

of the north path and mid-level vortices of the south path (Ross and Krishnamurti 2007, Hankes et al. 2015) generated independently or associated with a common AEW. The initiation of a vortex track at a given pressure level may also result from the vertical expansion of an already existing “primary” vortex. In this case, it is not really an initiation but just the point at which the vortex stretches vertically and remains vertically expanded for the following days. This "secondary" vortex initiation may for example result from vertical stretching related to the formation of MCSs and MCVs within a “primary” vortex. It may also result from the perturbation, possibly linked to orography, of the synoptic circulation near the primary vortex just before the actual vortex merging.

As shown in Chen and Liu (2014), the merger of a low-level dry vortex with a more intense mid-level moist vortex near the coast favors the cyclogenesis. The development of a mid-level vortex down to the surface generates frictional drag that may reinforce the low-level moisture convergence associated with the deep convection and favor cyclogenesis (Gray 1998). In addition, the vertical expansion of the Lagrangian recirculation (the “pouch”) in a vortex from the mid-troposphere to the boundary layer is important for cyclogenesis (Wang et al. 2012, Hankes et al. 2015). This vertical expansion may also appear well before cyclogenesis, as discussed in Thorncroft and Hodges (2001) and Hopsch et al. (2010) who showed that cyclogenetic vortices tend to extend at low-levels near the Fouta Djallon mountains (or Guinea highlands). This shows that the interannual cyclonic activity of the south path could be related in part to AEW characteristics near the coast, and not only to environmental conditions over the ocean (Gray 1968; DeMaria et al. 2001).

The orography may influence AEW initiation, either by its impact on the convective activity (see, e.g. Carlson 1969, Burpee 1972, Albignat and Reed 1980, Berry and Thorncroft 2005, Mekonnen et al. 2006, Mekonnen and Rossow 2018, Hamilton et al. 2020) or by its

impact in the setting up of a mean state favorable to their development (Wu et al. 2009, Hamilton et al. 2020). Orography can also promote vortex initiation by amplifying AEWs. Indeed, the deep convection triggered by the orography not only promotes the genesis of AEWs in East Africa, but also their intensification over West Africa (Hamilton et al. 2020). The role of orography on the dynamical initiation of dry vortices was explored by Mozer and Zehnder (1996a) using numerical simulations of a dry adiabatic flow. They showed that barotropic instabilities resulting from the blocking of the easterly flow by a mountain range can produce lee vortices that propagate downstream, in particular over West Africa (Mozer and Zehnder 1996b). A strengthening of low-level easterly winds (Harmattan) over the Hoggar mountains by an AEW could therefore favor the appearance of a vortex over West Africa. The potential role of the Hoggar mountains on the genesis of low-level vortices for the north path was also mentioned in Reed et al. (1988b) and in Thorncroft and Hodges (2001). Dry low-level vortices studied by Bou Karam et al. (2009) and that develop in the lee of Hoggar and Aïr mountains are also certainly related in part to AEWs of the north path.

A detailed description of the objective vortex tracking approach and of the datasets is given in section 2. Different aspects of the origin, the merging and the cyclogenesis of the vortices are analyzed in the following sections: initiation and track density in section3, seasonal and interannual variations in section 4, and longitudinal variations in section 5. Section 6 explores different types of vortex merging (confluence, expansion, local development) and their impact on cyclogenesis. The results are summarized and discussed in section 7.

2. Data and analysis

2.1. Vortex detection

The vortex tracking is done for 38 seasons (June to October) between 1980 and 2017 using ERA-Interim (ERA-I, Dee et al. 2011). This dataset has a horizontal resolution of 0.75° x 0.75° and a 6-hour time step. The vortex tracking is based on the geopotential height (ϕ) of a given pressure level (Duvel 2015, Duvel et al. 2017). The first step of this approach is to compute a geopotential height anomaly defined as the difference between ϕ and its average over a region of ±7.5° (i.e. ±10 ERA-I gridpoints). The "vortex area" is the ensemble of continuous grid points with a negative geopotential height anomaly and with an absolute value $\Delta\phi$ of this anomaly larger than a threshold $\Delta\phi_s$. To detect both weak and strong vortices while conserving a reasonable vortex size, $\Delta\phi_s$ varies between a minimum value $\Delta\phi_{min}$ adapted to weak depression, and a maximum value $\Delta\phi_{max}$ adapted to strong cyclonic depression. Technically, the threshold is increased from $\Delta\phi_{min}$ until it gives a vortex area with an equivalent radius lower than R_{max} = 4.2°. This value is a reasonable vortex size that allows a good overlap of the vortices between two timesteps. For the weakest vortices, the equivalent radius at $\Delta\phi_{min}$ must be larger than 1.2°. The threshold is chosen among an ensemble $\Delta\phi_s = \Delta\phi_{min} + s^2$ (where s is an integer $0 \leq s \leq 40$). The s^2 progression of the thresholds gives a better size adjustment capability for weak vortices.

2.2. Vortex track

A given vortex is tracked over time by considering the overlap (weighted by $\Delta\phi$) between vortex areas for two consecutive time steps. If several vortices overlap, the tracking uses the vortex with the largest overlap. The remaining vortices either start a new track generated by splitting or stop by "fusion". The positions of the vortex track are the barycenters of the vortex area computed considering all its gridpoints weighted by $\Delta\phi$. We

consider only vortices initiated in the domain 60°W-50°E and 0°N-30°N (Fig.1), but the tracking is done for a domain extending westward to 130°W and northward to 60°N. Since we are mostly interested in the cyclogenesis resulting from these vortices, we consider only vortices with a barycenter that spends at least one day over the Atlantic Ocean and that spends at least one timestep south of 20°N (in order to remove vortices that do not enter the MDR). Vortices that fulfill all these conditions are called Atlantic Vortices (AV) in the following sections.

2.3. Cyclogenetic vortices

If the barycenter of a vortex is located within 3° of an IBTrACS (Knapp et al. 2010) system (regardless of its intensity) for at least one timestep, it is considered a Cyclogenetic Atlantic Vortex (CAV), the others being therefore Non-CAV (NCAV). With this criterion, the match between the CAV and its IBTrACS system is longer than 1 day for 97% of the CAV and the average match is about 7 days. The first match generally corresponds to the first time-step of the IBTrACS system and is considered here as the CAV cyclogenesis point (see the example in Fig.1).

The CAV statistics was also used to refine the definition of $\Delta\phi_{min}$. CAV are indeed always detected when the corresponding TC appears over the ocean, whatever the value of $\Delta\phi_{min}$, but the initiation of the CAV may shift westward for large $\Delta\phi_{min}$. This is because a weak depression may break the vortex track and gives a new vortex downstream (i.e. westward). On the other hand, a too small $\Delta\phi_{min}$ produces many weak tracks of little interest, or even inconsistent structures in the geopotential anomaly field that reduces the number of AV. For this study, we use the two thresholds ($\Delta\phi_{min}$ = 40 m^2s^{-2} at 850 hPa and 50 m^2s^{-2} at 700 hPa) that maximize the number of CAV initiated over the continent. Using a larger $\Delta\phi_{min}$ (up to 80 m^2s^{-2}) decreases this number but this has no significant impact on the

conclusions given below, in particular on the average vortex distributions (spatial, seasonal) or on the relative impact of the North and the South path on cyclogenesis.

2.4. Merging between low-level and mid-level vortex tracks

A vortex track generally merges over the ocean with a vortex track of the other pressure level (e.g. Fig.1). The common parts of the tracks are detected by looking at pairs of 700 hPa and 850 hPa vortices having their barycenters located within 3° of each other. The first time this happens is the *merging time* between the two vortices and corresponds to the beginning of a vertically expanded vortex track that generally persists until vortex dissipation. It is thus possible to define a primary and a secondary vortex before merging, the primary being the older at merging time. If the secondary vortex is produced shortly before merging (e.g. <1 day), the merging corresponds to a *vertical expansion* of the primary vortex. In this case, the primary vortex initiation can be considered as the onset of the disturbance, e.g. the time at which a persistent closed circulation is formed near an AEW trough. If the secondary vortex is produced long before merging (e.g. ≥1 day), we may consider that the two vortices are formed "independently", while possibly related to a common synoptic or large-scale feature, and the merging corresponds to the *confluence* of the two vortex tracks (e.g. Fig.1). In this case, which roughly corresponds to the path merger studied in Hankes et al. (2015), the primary vortex is just the older one. AV initiated at the same time for both levels are counted as 700 hPa primary vortices.

2.5. Advantages and shortcomings of the tracking and merging algorithms

AEWs and their associated vortices are complex and intermittent features with perturbation patterns depending in particular on geographical location, pressure level and season. Different tracking algorithms based on different physical parameters, pressure levels and processing approach are thus susceptible to extract a different ensemble of cases. It is not

necessarily a problem if the results are interpreted considering the particularities of each algorithm. The vortex tracking approach used in this study is no exception to the rule. This algorithm is not designed to track all AEWs, in particular weak AEWs which are better targeted by dedicated algorithms such as those of Berry et al. (2007), Agudelo et al. (2011), Brammer and Thorncroft (2015) and Belanger et al. (2016). This algorithm detects the trough of the wave as soon as it is sufficiently developed to generate a persistent closed circulation (i.e. a detectable geopotential minimum). This is consistent with the approach of Thorncroft and Hodges (2001) but perhaps with a more precise vortex location because the geopotential field is naturally smoother than the vorticity field and does not require the use of low resolution. The adaptive threshold makes it possible to detect the vortex initiation at an early stage. However, vortex initiations are probably statistically shifted to the west compared to the initiation of the associated AEW since, as discussed above, a vortex is initiated only when the wave reaches a sufficient amplitude. This must be kept in mind when interpreting the results.

Regarding vortex merging, it should be noted that a vortex of the north path may coexist but not merge with a vortex of the south path. These vortices are classified as non-mergers by the algorithm while they are theoretically part of the same perturbation. Some low-level vortices on the north path are therefore not considered to be cyclogenetic whereas they can influence cyclogenetic vortices of the south path via a modification of the environmental flow (e.g., Brammer and Thorncroft 2015, 2017). These cases are probably not very frequent as the two paths generally merge over the ocean (e.g. Reed at al 1988a, 1988b, Diedhiou et al. 1999, Thorncroft and Hodges 2001, Ross and Krishnamurti 2007).

For some mature AEWs, the mid-level vortex of the south path may first expand downward and then merge with a low-level north path vortex, temporally forming a system with one mid-level vortex and two low-level vortices (e.g., Carlson 1969; Berry and Thorncroft 2005). The couple of low-level vortices generally join over the ocean west of the Guinea highlands. The algorithm considers those cases, but associates the mid-level track with either the north or the south low-level track (quite randomly since it is based on the vortex overlap at "fusion" time, see above). The other low-level track becomes either a non-merging AV or is eliminated if it does not fulfil the AV criteria before fusion. As shown in Ross and Krishnamuri (2007), such fusion between *low-level* vortex tracks near the coast is the exception rather than the rule.

3. Vortex initiation and track density

3.1. All Atlantic vortices

Over West Africa, AV are initiated mostly north of 15°N at 850 hPa and south of 15°N at 700 hPa (Fig.2a and 2b). At 700 hPa (Fig.2a), AV initiations are maximal at 10°N and west of the Fouta Djallon mountains in agreement with previous results (e.g., Thorncroft and Hodges 2001, Berry and Thorncroft 2005, Chen 2006, Hopsch et al. 2010). This is likely associated with AEW reinforcement by latent heat release in organized deep convection that generally develops in the lee side of high terrain (Laing et al. 2008). There are two secondary maxima at 5°E and 30°E that are located east of the Cameroon and the Ethiopian highlands (only results west of 30°E are shown to focus on regions with large AV density). At 850 hPa (Fig.2b), AV initiations are clearly related to the orography with a large maximum centered west of Hoggar mountains (5°E, 24°N) and a secondary maximum centered west of Tibesti mountains (16°E, 20°N). This relation with orography is

clearer than in previous studies, probably because of the larger and more persistent impact of orography on geopotential compared to vorticity. The precise physical origin of these AV initiations is not studied in this paper. They are not necessarily the signature of AEW initiations, but they do show the influence of orography in forming persistent low-level closed circulations that propagates westward to the ocean. For the 38 seasons (JJASO), the number of AV initiated in our domain (60°W to 50°E) is comparable for both pressure levels (~1700 or about 45 by season). More details are given below for initiation density maps of non-merging AVs (Fig.3), merging non-cyclogenetic AVs (NCAV, Fig.4), and cyclogenetic AVs (CAV, Fig.5).

3.2. Non-Merging Atlantic vortices

Non-merging AVs are disturbances with no persistent vertical expansion and they are generally not cyclogenetic. Initiations of non-merging AV (Fig.3) are more evenly distributed over the domain compared to the AV ensemble, with a relatively higher density over the Atlantic Ocean. In fact, vortices initiated over land and reaching and staying over the ocean for at least one day have certainly more chance to be stronger vortices since the weaker ones will dissipate before reaching the ocean. On the contrary, AV generated over the ocean can be short-lived systems (i.e. 1 day). This fact certainly contributes to increase the proportion of weak non-merging and non-cyclogenetic AVs over the ocean. At 700 hPa (Fig.3a), a particular pattern is underlined in the northwest sector of the domain with AV generated north of 15°N at mid-level and that propagate southwestward over the ocean. These mid-level vortices are probably linked to the Moroccan vortex (Cheng et al. 2019) generated by the interaction between the AEW and the basic-state potential vorticity gradient.

3.3. Non-cyclogenetic Atlantic vortices (NCAV)

Mid-level primary NCAVs (Fig.4a) are mainly initiated around 10°N over the ocean west of Guinea highlands and over land west of Cameroon highlands and Jos Plateau. Only a few low-level secondary NCAVs are initiated at 10°N and may correspond to local downward expansion of mid-level vortices. Low-level secondary NCAVs (Fig.4c) are mainly initiated around 15°N over the ocean and thus north of the mid-level vortex track (see Fig.6) and the merger occurs mostly near 20°W (Fig.4e). These mergers may correspond to dry vortex mergers studied in Chen and Liu (2014). Low-level primary NCAVs (Fig.4b) are mainly initiated near the Hoggar mountains and have thus a totally different density pattern compared to low-level secondary NCAVs (Fig.4c). These primary vortices do not dissipate over the ocean, but rather merge west of 20°W (Fig.4f) with mid-level vortices initiated mostly to the west of the Guinea highlands (Fig.4d). The maximum merging density (Fig.4e and 4f) is shifted west by only a few degrees compared to the maximum initiation density of secondary NCAV. This shows that the merging occurs generally shortly after the initiation of the secondary vortex and may therefore be considered as a vortex deepening, even if the secondary vortex is initiated at some distance from the primary vortex track. However, among the secondary vortices initiated over the continent east of 10°W, some are initiated south of 15°N at 700 hPa (Fig.4d) and north of 15°N at 850 hPa (Fig.4c) while there is no *local* primary vortex counterpart. This reveals initiations of independent north and south vortex tracks that will later merge by *confluence* (see section 6).

3.4. Cyclogenetic Atlantic Vortices (CAV)

Figure 5a suggests that there are relatively more CAV initiated over the continent. The ratio between initiations occurring east and west of 10°W is indeed 1.5 times greater for the CAV compared to NCAV. This shows that AEWs that develop a vortex further east at

301 the jet level have more chance to be cyclogenetic. Many secondary low-level CAV are also
302 initiated (Fig.5c) and merge (Fig.5e) over the continent, in good agreement with previous
303 studies showing that cyclogenetic AEWs generally extend at low-levels over the continent
304 (see section 5.2). For CAV, maximum initiation and merging are both on the coast near
305 10°N, suggesting a large influence of deep convection on the vertical expansion. This
306 downward expansion is also more distributed in longitude for CAV compared to NCAV.
307 Some secondary vortices appear west of 30°W over the ocean (Fig.5c), corresponding to
308 late downward expansion and cyclogenesis. A more detailed analysis (not shown) reveals
309 that : (i) the maximum cyclogenesis west of 20°W (Fig.5g) is related to downward expan-
310 sion near the coast and over West Africa along 10°N and (ii) that the smaller cyclogenesis
311 maximum west of 30°W is related to secondary CAV initiated (Fig.5c) north of 15°N near
312 20°W.

313 Low-level primary CAV initiations (Fig.5b) are more frequent near the Hoggar mountains,
314 but there are also some initiations near 10°N over West Africa showing that cyclogenetic
315 low-level vortices may lead slightly mid-level ones on the south-path. Mid-level secondary
316 CAV are initiated mainly near the coast, around 35°W and west of 50°W (Fig.5d). Those
317 formed over the ocean merge rapidly and correspond to a local upward expansion of the
318 low-level vortices (Fig.5f) shifted westward for CAV compared to NCAV. Cyclogenesis of
319 vortices initiated near Hoggar and Tibesti mountains is also shifted westward compared
320 to the cyclogenesis of vortices initiated at the jet level, with a weak cyclogenesis near
321 25°W (Fig.5h). This agrees with the results of Chen et al. (2008) showing that disturb-
322 ances of the north path take longer to initiate a TC.

323 Compared to the NCAV ensemble, CAV have a more variable initiation distribution for
324 both primary and secondary vortices. While most NCAV mergers occur near the coast just

west of 20°W (Fig.4e and 4f), CAV mergers occur either further west over the ocean or over land and at the coast for downward expansion of mid-level vortices (Fig.5e). This suggests that there are specific or favorable processes for the vertical expansion of the vortices before cyclogenesis over these regions, related for example to pouch formation over the ocean and to the development of deep convection over land.

3.5. Initiation and cyclogenesis statistics

A summary of the distribution of primary AV initiations and of their influence on cyclogenesis is reported in table 2. Summing all primary AVs initiated over the north and the south path domains, there are 938 initiations and thus about 25 by season (JJASO) (Table 2a). As expected, because we detect only developed AEWs, this is small compared to the 43 AEWs initiated over West Africa per season (JJAS) in Chen (2006) and the 61 AEWs per season (MJJASON) in Avila et al. (2000) that suggest a quite continuous wave activity with more than one trough crossing the coast every 3 or 3.5 days. Compared to the present analysis, Chen (2006) found a more comparable number of initiations for the south path (~13 by seasons), but a larger number of initiations for the north path (~30 by season), suggesting that a larger proportion of weak AEWs are not selected by our approach for the north path.

About 23% of primary AV initiated on the south path are cyclogenetic compared to only 10% on the north path (Table 2b). For the 38 hurricane seasons, there are 305 IBTrACS systems (about 57% of the total number of North Atlantic systems) initiated south of 20°N, 217 in the MDR and 88 west of 60°W. Over the MDR, 16% of the cyclogenesis is due to low-level primary AV of the north path and 38% to mid-level primary AV of the south path (Table 2c). In total, 62% of the MDR cyclogenesis is due to primary AV initiated east of 10°W at both pressure levels. However, this percentage drops to 30% of the entire

North Atlantic cyclogenesis. This is half of the cyclogenesis due to AEWs found in previous studies (e.g. Avila et al. 2000, Chen et al. 2008, Russel et al. 2017) using a subjective AEW detection. This suggests that about half of these cyclogenetic AEWs are associated with a vortex initiated east of 10°W, the remainder being mainly initiated near the coast (Fig. 5a).

Only 38% of the MDR cyclogenesis is due to primary AV initiated locally over the Atlantic Ocean and coastal regions at either 700 hPa (20%) or 850 hPa (18%) (Table 2c). These primary AV are more numerous compared to continental primary AV, especially at 700 hPa where there is a large concentration near the coast (Fig.4a and 5a), but they have a weak cyclogenesis efficiency (9% at 700 hPa and 11% at 850hPa) (Table 2b). West of 60°W and south of 20°N (Table 2d), only 37% of the cyclogenesis is associated with AV coming from eastern regions: 12% from the continent and 25% from the Atlantic Ocean and coastal regions. This shows that cyclogenesis occurring far from the West African coast have logically little chance to be associated with a persistent vortex initiated over West Africa or near the coast (see also section 5).

3.6. Track density

A track density map gives the probability of presence of a vortex of a given type. The track density is maximal around 25°W for both levels and for all NCAV types (Fig.6). This is due to the superposition of AVs just initiated near the coast and those initiated over the continent and not yet dissipated over the ocean. The speed of the vortex barycenters also tends to slow down and thus to increase the vortex occurrence at these longitudes (not shown). For non-merging NCAV (Fig.6a and 6b) this probability is smaller compared to primary merging NCAV (Fig.6c and 6d), mostly because of their shorter duration. There is no clear gap in the NCAV track density near the coast. Low-level vortices initiated near

373 the Hoggar mountains follow quite continuously a west-southwestward trajectory and
374 mid-level vortices initiated south of the AEJ follow quite continuously a west-northwest-
375 ward trajectory. Secondary NCAV (Fig.6e and 6f) have a smaller track density, not only
376 over West Africa, but also over the ocean because of their later development.

377 At 700 hPa, primary CAV track density (Fig.7a) grows east-northeastward from West Af-
378 rica with a maximum density at 25°W and a large track density until the western bound-
379 ary. As expected, associated secondary track density at 850 hPa is smaller over the conti-
380 nent and is maximal further west over the ocean (Fig.7c). The track density of primary
381 CAV at 850 hPa (Fig.7b) is very different with a maximum shifted southwestward near
382 40°W over the ocean. There is a weak south-path track associated with low-level primary
383 CAV initiated over West Africa. At 15°W, the maximum track density jumps from 20°N to
384 15°N, suggesting a discontinuity of AV tracks near the coast for CAV. This is not due only
385 to primary vortices initiated near the coast. Low-level CAV initiated near the Hoggar
386 mountains have indeed a similar track density pattern (not shown) and are thus not dis-
387 sipated near the coast. This discontinuity may be associated with the feature described in
388 Chen and Liu (2014) that intense AEWs tend to shift dry low-level vortices southwest-
389 ward before favoring cyclogenetic merge with a mid-level vortex.

390 ## 4. Seasonal and interannual variation

391 Previous analyses (e.g., Duvel 1990; Thorncroft and Hodges 2001; Hopsch et al. 2007;
392 Ross and Krishnamurti 2007) generally found that north path activity is larger at the be-
393 ginning of the season and south path activity at the end of the season (August and Sep-
394 tember). As shown in figure 8, this seasonal variation is mostly related to the number of
395 primary merging AV initiations (N_{AV}) over West Africa (Fig.8b) which is maximum in July

at 850 hPa and in August at 700 hPa. Since primary AV at 850 hPa are mostly initiated near Hoggar mountains (Fig.4b and 5b), this illustrates the large efficiency of these orographic processes at the start of the hurricane season. For both pressure levels, the number of primary CAV initiations (N_{CAV}) over West Africa is small in July, maximal in August, and decreases for the following months. AVs initiated near the coast (Fig.8a) and non-merging AV (Fig.8c and 8d) have a weak seasonal variation. For coastal regions (Fig.8a), N_{AV} is more evenly distributed along the season with values of about 1 per month at 700 hPa and 0.5 per month at 850 hPa.

The cyclogenesis efficiency (CE = N_{CAV}/N_{AV}) of primary AV initiated over West Africa is maximal in August (~30%) and small in July (<10%) for both paths (Fig.9a). Both paths have thus an equivalent CE for July and August. This is consistent with Agudelo et al. (2011) who showed that about 80% of the seasonal cycle of CE is determined by the large-scale environment over the ocean that is optimal in August and September (Emanuel and Nolan 2004, Tippet et al. 2011, Menkes et al. 2011). The low average CE for the north path (10%) in table 2b is thus mostly due to its unfavorable seasonal phase with maximum vortex initiations in July. According to previous results (e.g. Duvel 1990, Ross and Krishnamurti 2007), AEW amplitude and low-level vorticity near the coast is also maximal in August-September, that could explain part of the relation between south path vortices intensity and cyclogenesis.

The Merging Efficiency (ME) index that is just the proportion of merging AV represents the ability of the vortices to deepen and could be also related to the cyclogenesis. The ME for primary AV initiated over West Africa (Fig.9b) has however high values for the north path between June and August with no correlation with CE. Nevertheless, the smaller ME in September at 850 hPa may be at the origin of the corresponding smaller CE. This shows

that the vertical deepening of a vortex is a necessary but not a sufficient condition for cyclogenesis and that a larger ME does not necessarily lead to a larger CE at the seasonal time scale.

Primary AVs initiated in August and September over West Africa have an averaged CE of 26% that agrees well with the value found by Agudelo et al. (2011). This CE is however very variable from one year to another (Fig.9c). This suggests that the cyclogenesis does not depend on the *number* of AVs initiated over the continent during the active season. According to Agudelo et al. (2011), about half of the interannual variability of the cyclogenesis may be attributed to variations of the large-scale environment. Our result suggests that the remaining part is not due to the *number* of AV generated over West Africa, but rather to vortex intensification due to more local and stochastic process (such as the development of MCSs and MCVs).

5. Longitudinal variations of cyclogenesis

5.1. Impact of the CAV origin on the cyclogenesis longitude

The average number of cyclogenesis is quite evenly distributed with longitude (Fig.10). However, the CAV origin (West Africa, coast or open ocean) strongly depends on the cyclogenesis longitude. Vortices initiated over West Africa are the main contributor for the MDR cyclogenesis (62% on average, Table 2c) with a cyclogenesis fraction that gradually decreases from 80% near the coast to about 30% at 60°W. The large fraction near the coast may be due to the fact that many AV initiated over West Africa are already strong and vertically developed when arriving over the ocean. These vortices increase low-level convergence and possibly create a "pouch" effect (Dunkerton et al. 2009) that may promote deep convection and cyclogenesis near the coast. The comparison of figures 5g and

443 5h shows that most of the cyclogenesis near the coast is due to the moist mid-level CAVs
444 of the south path and not to the dry low-level CAVs of the north path that take more time
445 to trigger cyclogenesis. The cyclogenesis fraction due to CAV initiated over the ocean in-
446 creases from zero at 20°W to about 40% at 60°W. Such CAV initiation and intensification
447 over the ocean may be related to local development of organized deep convection, possi-
448 bly triggered by weak AEWs formed further east over West Africa. By contrast, the cyclo-
449 genesis fraction due to primary AV initiated near the coast is quite constant with longi-
450 tude (~20%), probably because it mixes the process of the two other regional sources of
451 CAV.

452 *5.2. Vortex intensity and vortex merging*

453 The impact of vortex intensity on CE may be studied by comparing average CAV and NCAV
454 intensity as a function of longitude or relative to merging time. For the south path at 700
455 hPa (Fig.11a), the primary NCAV intensity is relatively constant with longitude with a
456 slight increase west of 0°E and a slight decrease over the ocean. This agrees with the av-
457 erage growth rate reported in Thorncroft and Hodges (2001). As expected, the CAV inten-
458 sity is larger and increases westward over the ocean, mostly because of the increasing TC
459 proportion and TC strength. An interesting point is that CAV intensity is also significantly
460 larger between 5°W and the coast (Fig.11a), showing that AV having a large intensity over
461 the continent are more likely to be cyclogenetic. This is compatible with Hopsch et al.
462 (2007) who showed that AEW variance near the coast is positively correlated with the
463 number of TCs at interannual time-scale. This also agrees with previous studies (Thorn-
464 croft and Hodges 2001, Hopsch et al, 2010, Agudelo et al. 2011, Arnault and Roux 2011,
465 Brammer and Thorncroft 2015) showing that characteristics of the AEW trough (low-
466 level vorticity, column humidity, vertical velocity and other parameters related to deep
467 convection) between 0°E and the coast have an influence on further wave development

and cyclogenesis. Other features such as the effect of consecutive AEW troughs (Dieng et al. 2017) may also have an influence on AEW development near the coast. The intensity of north path NCAV (Fig.11b) is larger over land at 850 hPa compared to 700 hPa. While this intensity decays strongly near the coast, as noticed by Thorncroft and Hodges (2001), it remains stronger or equal to the NCAV intensity of the south path for all longitudes. Although less significant than at 700 hPa, there is also a tendency for a larger CAV intensity near the coast at 850 hPa.

The downward deepening of 700 hPa vortices is associated with a transitory intensification for both CAV and NCAV (Fig.11c). The upward deepening of 850 hPa vortices corresponds to a pause in an intensity decrease over the previous 2 days (Fig.11d). The CAV intensity becomes significantly larger than the NCAV intensity about 36 hours after vortex deepening, partly because of the progressively greater TC occurrence westward. Cyclogenesis generally occurs after vortex deepening (Fig.11c and 11d) with most probable delay around two days, but cyclogenesis can occur up to 10 days after vortex deepening. The consistent timing between the deepening and the cyclogenesis demonstrates the remarkable agreement between IBTrACS and the vortex dynamics in ERA-I.

6. Different types of vortex merging

The previous sections present the difference between primary and secondary vortices, but with no consideration of the delay between initiation and merging. However, the nature of the merging can be interpreted differently depending on this delay. Four merging categories are illustrated in Fig.12 based on the merging types described in section 2.4. The first category (Fig.12a) corresponds to the *confluence* of two vortex tracks. The second category (Fig.12b) corresponds to a local development of the depression, related for

example to MCSs, with delay ≤1 day between initiation and merging for both levels. The next two categories (Fig.12c and 12d) correspond to a delay between initiation and merging > 1 day for the primary vortex and ≤1 day for the secondary vortex. This is interpreted as a vertical expansion of the primary vortex. The 1-day threshold is somewhat arbitrary among reasonable values (say between 12 h and 2 days). It is chosen because it gives a relatively homogeneous distribution of the four merging categories (between 21% and 30%) and it makes it possible to identify quite clearly the source of the vortices for each category (Fig.13).

For merging happening more than one day after vortex initiations at both levels, initiation density maps clearly reflect the north and the south paths over the continent and near the coast (Fig.13a). This "confluence" category represents 25% of the mergers, with 15% initiated east of 10°W and 10% initiated near the coast. The shift of the merging densities between the two pressure levels (Fig.14a) shows that the low-level vortex is located northwest and therefore slightly ahead of the mid-level vortex at merging time. This merging category is associated with 23% of the cyclogenesis, mostly east of 30°W. These mergers peak in July and August (Fig.15a) and give a CE of about 20% in August and September that agrees with the value found by Hankes et al. (2015) for a similar definition of the confluence of north and south path vortices (but not identical since they consider only cyclogenesis east of 40°E).

Initiation density maps for fast merging vortices (Fig.13b) is concentrated offshore, west of the Guinean coast, for both levels. As expected for these fast mergers that corresponds to a local vortex development, initiation (Fig.13b) and merging (Fig.14b) density maps are quite similar. These fast merging vortices are associated with 24% of the cyclogenesis,

514 with a clear maximum for occurrence and CE in September (Fig.15b). Downward deepen-
515 ing of primary 700 hPa vortices (Fig.13c) concerns mostly mid-level vortices initiated
516 over the continent, those initiated offshore west of the Guinean coast being fast mergers
517 (Fig.13b). Only a few mid-level vortices expand downward over the continent, mostly
518 near the Guinea highlands. The most part expands downward by merging with low-level
519 vortices initiated over the ocean around 15°N (Fig.13c and 14c). This category represents
520 the largest amount of cyclogenesis (37%), mostly near the coast, with a peak activity in
521 August and September (Fig.15c). Upward deepening of primary 850 hPa vortices
522 (Fig.13d) concerns mostly low-level vortices initiated west of the Hoggar and Tibesti
523 mountains. A few of these vortices expand early over the continent, but most of them ex-
524 pand over the ocean near 20°W by merging with mid-level vortices initiated west of the
525 Guinea highlands (Fig.13d and 14d). The mid-level vortices are clearly located south of
526 the low-level vortices at merging time (Fig.14d), suggesting that these mid-level vortices
527 are induced by the synoptic dynamical perturbation of a low-level vortex and not by deep
528 convection developing into the low-level vortex. This category is relatively frequent
529 (24%), but represents only 16% of the cyclogenesis. This is mostly due to the fact that
530 these mergers peak in July (Fig.15d) when the MDR cyclogenesis potential index related
531 to the large-scale environment is weak. Note that CE is large in September for this merging
532 category compared to the ensemble of low-level primary AV (Fig.9a) that includes non-
533 mergers.

7. Conclusions

7.1. Importance of distinguishing primary and secondary vortices

This study shows the importance of considering at least two pressure levels, one in the low-level monsoon and Harmattan flows (850 hPa) and one in the AEJ (700 hPa), in order to take into account the complexity of vortex initiation processes over West Africa. Figures 4 and 5 shows that many vortex tracks initiated near the coast or over the Atlantic Ocean result from a vertical expansion of primary vortices initiated over West Africa where they follow very distinct paths depending on the pressure level. As illustrated in figures 13a and 14a, about 25% of mergers are confluences between north and south path vortices initiated independently over West Africa (such as the case shown in figure 1) or near the coast. For the "expansion" categories c and d and even for the "local development" category b, the merging does not generally occur at the same place as the initiation of the secondary vortex (Fig. 13 and 14). This suggests that some secondary vortices do not develop vertically from the primary vortex, but nearby due to the dynamic influence of this primary vortex. This can be for example the case for the dry low-level vortices that are associated with mid-level vortices described in Chen and Liu (2014) and that have a signature near 15°N in figures 4c, 5c, 13a and 13c.

In agreement with Chen (2008), merging categories involving the north path tend to delay the cyclogenesis to the west. The vortex deepening associated with merging is a necessary but not a sufficient condition for cyclogenesis. The deepening tends to increase the vortex strength, especially for mid-level primary vortices (Fig.11c), but this is generally not sufficient for cyclogenesis. The cyclogenesis efficiency increases for vortices that deepen

556 over West Africa or near the coast, but it also largely depends on environmental condi-
557 tions, as discussed above. Cyclogenesis occurs more often about two days after deepening,
558 but it can be delayed for up to 10 days.

559 *7.2. Seasonal and Interannual variations of continental primary vortices*

560 The number of primary vortices produced on the north path is maximal in July and grad-
561 ually decreases in August and September. For the south path, this number is maximal in
562 August and September. Since the cyclogenetic potential index of the MDR is far larger in
563 August and September compared to July, the south path is more efficient for cyclogenesis
564 (23% of CAV) compared to the north path (10% of CAV). However, the cyclogenetic effi-
565 ciency is about 30% for both paths in August, suggesting that low-level north path vorti-
566 ces are nearly as efficient as mid-level south path vortices when the cyclogenesis potential
567 index is high. The interannual variation of the total *number* of AV produced in August and
568 September over West Africa is not correlated with the cyclogenesis. This suggests that
569 seasonal and interannual modulations of the cyclogenesis over the North Atlantic is re-
570 lated more to large-scale environmental conditions than to the *number* of vortices cross-
571 ing the West African coast. This is not a common tendency for other basins and time-
572 scales. For example, the MJO modulation of cyclogenesis over the Indian Ocean is more
573 linked to the number of vortices than to the intensification of these vortices (Liebman et
574 al. 1994, Duvel 2015). For the Atlantic Ocean, the weak impact of the number of vortices
575 can be tentatively attributed to the large and sustained number of vortices produced over
576 West Africa and near the coast during the whole season. These numerous vortices may
577 seed cyclogenesis over the MDR as soon as local environmental conditions are favorable.
578 As shown in figure 10, this process is however mostly valid near the coast and is progres-
579 sively replaced toward the west by local vortex initiations due for example to MCS organ-

ization or to AEWs reaching a critical layer. Patricola et al. (2018) showed that the cyclogenesis frequency is maintained in a climate model if the AEWs are suppressed. This is because the model generates TCs by other mechanisms. In nature, however, it is possible that the cyclogenesis will be reduced, especially near the coast, if the AEW activity decreases significantly. This will be the case if the development of a local vortex is not as efficient for cyclogenesis as the triggering by an already closed circulation coming from West Africa. In such a case, the excess of convective instability (and ocean heat content) could be released gradually by a succession of MCSs rather than rapidly by a single TC. In global warming simulations, current GCMs indicate an increase in the north path intensity and a decrease of the south path intensity (Skinner and Diffenbaugh 2014, Hannah and Aiyyer 2017, Kebe et al. 2020). Brannan and Martin (2020) also showed a shift of the south path amplitude toward the end of the season. These changes may influence the longitudinal distribution of the cyclogenesis and the average cyclogenesis by modifying the seasonal phase of the AEW activity.

7.3. North path and orography

This analysis clearly shows the fundamental influence of the Hoggar mountains on the initiation of persistent dry vortices of the north path. This agrees with the recent study of Hamilton et al. (2020) who showed, using a high-resolution model, that the wave kinetic energy at low-level is reduced north of 15°N over West Africa when the orography is reduced or removed. Previous results of Mozer and Zehnder (1996b), while based on a coarser resolution and simplified dry model, give interesting additional information on this vortex genesis process. In their model the easterly flow is blocked by the Hoggar mountains and forms a low-level jet primarily to the south. When the simulation starts, a vortex develops west of the Hoggar mountains as a transient disturbance that moves

downstream. The dry vortex genesis region west of the Hoggar mountains could thus result from episodic reinforcements of the northeastern wind (Harmattan), related for example to intraseasonal pulsation of the West African heat low (Lavaysse et al. 2010), that would cause the development of such transient disturbances. This agrees with a hypothesis of Chen (2006) that the baroclinic instability at low-levels may be triggered by the intrusion of dry northerlies and transported westward by the Harmattan. This also agrees with Thorncroft and Rowell (1998) who showed a positive correlation between the strength of the easterly low-level wind and the AEW activity in a GCM, possibly due to the resulting stronger interaction with the orography. Further analysis using the vortex dataset obtained here and ECMWF re-analysis could provide an interesting assessment of the role of these orographic processes on the origin of the dry north path vortices.

Acknowledgments: ECMWF ERA-Interim data used in this study have been obtained from the ECMWF data server and processed on the IPSL mesocenter ESPRI facility which is supported by CNRS, UPMC, Labex L-IPSL, CNES and Ecole Polytechnique. The International Best Track Archive for Climate Stewardship (IBTrACS) data has been obtained from the NOAA NCDC web site.

627 REFERENCES

628 Agudelo, P., C. D. Hoyos, J. Curry, and P. J. Webster, 2011: Probabilistic discrimination be-
629 tween large-scale environ- ments of intensifying and decaying African easterly waves. *Cli-*
630 *mate Dynamics*, **36**, 1379–1401.

631 Albignat, J. P., and R. J. Reed, 1980: The origin of African wave disturbances during Phase
632 III of GATE. *Mon. Wea. Rev.,* **108,** 1827–1839.

633 Arnault, J., and F. Roux, 2011: Characteristics of African easterly waves associated with
634 tropical cyclogenesis in the Cape Verde Islands region in July–August–September of
635 2004–2008. *Atmos. Res.*, **100**, 61–82.

636 Avila, L. A., R. J. Pasch, and J.-G. Jiing, 2000: Atlantic tropical systems of 1996 and 1997:
637 Years of contrasts, *Mon. Wea. Rev.*, **128**, 3695 – 3706.

638 Belanger, J. I., M. T. Jelinek, J. A. Curry, 2016: A climatology of easterly waves in the tropical
639 Western Hemisphere. *Geosci. Data J.*, **3**, 40–49.

640 Berry, G., and C. D. Thorncroft, 2005: Case study of an intense African easterly wave. *Mon.*
641 *Wea. Rev.*, **133,** 752–766.

642 Berry, G., C. D. Thorncroft and T. Hewson, 2007: African easterly waves during 2004 -
643 Analysis using objective techniques. *Mon. Wea. Rev.*, **135**, 1251–1267.

644 Bou Karam, D., C. Flamant, P. Tulet, M. C. Todd, J. Pelon, and E. Williams, 2009: Dry cyclo-
645 genesis and dust mobilization in the intertropical discontinuity of the West African Mon-
646 soon: A case study, *J. Geophys. Res.*, **114**, D05115.

647 Brammer, A., and C. D. Thorncroft, 2015: Variability and evolution of African easterly
648 wave structures and their relationship with tropical cyclogenesis over the eastern Atlan-
649 tic. *Mon. Wea. Rev.*, **143**, 4975–4995.

650 Brammer, A., and C. D. Thorncroft, 2017: Spatial and temporal variability of the three-
651 dimensional flow around African easterly waves. *Mon. Wea. Rev.*, **145**, 2879–2895.

652 Brannan, A. L., and E. R. Martin, 2019: Future characteristics of African Easterly Wave
653 tracks. *Climate Dynamics*, **52**, 5567–5584.

654 Burpee, R. W., 1972: The origin and structure of easterly waves in the lower troposphere
655 of North Africa. *J. Atmos. Sci.*, **29**, 77– 90.

656 Carlson, T. N., 1969: Synoptic histories of three African disturbances that developed into
657 Atlantic hurricanes. *Mon. Wea. Rev.*, **97,** 256–276.

658 Cecelski, S. F., and D.-L. Zhang, 2013: Genesis of Hurricane Julia (2010) within an African
659 easterly wave: Low-level vortices and upper-level warming. *J. Atmos. Sci.*, **70**, 3799–3817.

660 Chen T-C., 2006: Characteristics of African easterly waves depicted by ECMWF reanalyses
661 for 1991–2000. *Mon. Wea. Rev.,* **134**, 3539–3566.

662 Chen T. C., S-Y. Wang, and A. J. Clark, 2008. North Atlantic hurricanes contributed by Afri-
663 can easterly waves north and south of the African easterly jet. *J. Climate*, **21**, 6767–6776.

664 Chen, S.-H., and Y.-C. Liu, 2014: The relation between dry vortex merger and tropical cy-
665 clone genesis over the Atlantic Ocean, *J. Geophys. Res. Atmos.*, **119**, 11,641–11,661.

666 Cheng, Y. M., C. D. Thorncroft, and G. N. Kiladis, 2019: Two contrasting African easterly
667 wave behaviors. *J. Atmos. Sci.*, **76**, 1753-1768.

668 Dee, D.P., and co-authors, 2011: The ERA-Interim reanalysis: Configuration and perfor-
669 mance of the data assimilation system. *Quart. J. Roy. Meteor. Soc.*, **137**, 553–597.

670 DeMaria, M., J. A. Knaff, and B. H. Conell, 2001: A tropical cyclone genesis parameter for
671 the tropical Atlantic. *Wea. Forecasting,* **16,** 219–233.

672 Diedhiou, A., S. Janicot, A. Viltard, P. de Félice, and H. Laurent, 1999 : Easterly waves re-
673 gimes and associated convection over West Africa and the tropical Atlantic: results from
674 the NCEP/NCAR and ECMWF reanalyses. *Climate Dynamics*, **15**, 795 - 822.

675 Diedhiou, A., Janicot, S., Viltard, A., and P. de Felice, 2002: Energetics of easterly wave dis-
676 turbances over West Africa and the tropical Atlantic: A climatology from 1979-95
677 NCEP/NCAR reanalyses. *Climate Dynamics*, **18**, 487–500.

678 Dieng, A. L., S. M. Sall, L. Eymard, M. Leduc-Leballeur, and A. Lazar, 2017: Trains of African
679 easterly waves and their relationship to tropical cyclone genesis in the eastern Atlantic.
680 *Mon. Wea. Rev.*, **145**, 599 – 616.

681 Dunkerton, T. J., M. T. Montgomery, and Z. Wang, 2009: Tropical cyclogenesis in a tropical
682 wave critical layer: Easterly waves. *Atmos. Chem. Phys.*, **9**, 5587–5646.

683 Duvel, J. P., 1990: Convection over tropical Africa and the Atlantic Ocean during northern
684 summer. Part II: Modulation by easterly waves. *Mon. Wea. Rev.*, **118**, 1855–1868.

685 Duvel, J. P., 2015: Initiation and Intensification of Tropical Depressions over the Southern
686 Indian Ocean: Influence of the MJO. *Mon. Wea. Rev.*, **143**, 2170–2191.

687 Duvel, J.P., S.J. Camargo and A.H. Sobel, 2017: Role of the Convection Scheme in Modeling
688 Initiation and Intensification of Tropical Depressions over the North Atlantic. *Mon. Wea.*
689 *Rev.*, **145**, 1495-1509.

690 Emanuel, K.A., and D.S. Nolan, 2004: Tropical cyclone activity and global climate. In: Pro-
691 ceedings of 26th conference on hurricanes and tropical meteorology. *American Meteoro-*
692 *logical Society*, Miami, FL, pp 240–241.

693 Erickson, C. O., 1963: An incipient hurricane near the West African coast. *Mon. Wea. Rev.*,
694 **91**, 61-68.

695 Fink, A. H., and A. Reiner, 2003: Spatio-temporal variability of the relation between Afri-
696 can easterly waves and West African squall lines in 1998 and 1999. *J. Geophys. Res.*, **108**,
697 4332.

698 Gray, W. M., 1968: Global view of the origin of tropical disturbances and storms. *Mon. Wea.*
699 *Rev.,* **96,** 669–700.

700 Gray, W. M., 1998: The formation of tropical cyclones. *Meteor. Atmos. Phys.*, **67**, 37–69.

701 Hamilton, H. L., Núñez Ocasio, K. M., Evans, J. L., Young, G. S., and J. D. Fuentes, 2020: Topo-
702 graphic influence on the African Easterly Jet and African Easterly Wave energetics. *J. Ge-*
703 *ophys. Res.: Atmospheres*, **125**, e2019JD032138.

704 Hannah, W. M., and A. Aiyyer, 2017:. Reduced African Easterly Wave Activity with Quad-
705 rupled CO2 in the Superparameterized CESM. *Journal of Climate*, 30(20), 8253– 8274.

706 Hankes, I., Z. Wang, G. Zhang, and C. L. Fritz, 2015: Merger of African easterly waves and
707 formation of Cape Verde storms. *Quart. J. Roy. Meteor. Soc.*, **141**, 1306–1319.

708 Hodges, K. I., 1995: Feature tracking on the unit sphere. *Mon. Wea. Rev.*, **123**, 3458–3465.

709 Hodges, K. I., 1999: Adaptive constraints for feature tracking. *Mon. Wea. Rev.*, **127**, 1362–
710 1373.

711 Hodges, K. I., B. J. Hoskins, J. Boyle, and C. Thorncroft, 2003: A comparison of recent rea-
712 nalysis datasets using objective feature tracking: Storm tracks and tropical easterly
713 waves. *Mon. Wea. Rev.*, **131**, 2012–2037.

714 Hopsch S. B., C.D. Thorncroft, K. Hodges and A. Aiyyer, 2007: West African storm tracks
715 and their relationship to Atlantic tropical cyclones. *J. Climate* **20**: 2468 – 2483.

716 Hopsch S. B., Thorncroft C. D. and K. R. Tyle, 2010: Analysis of African Easterly wave struc-
717 tures and their role in influencing tropical cyclogenesis. *Mon. Wea. Rev.*, **138**, 1399–1419.

718 Kebe, I., I. Diallo, M. B. Sylla, F. De Sales, and A. Diedhiou, 220: Late 21st Century Projected
719 Changes in the Relationship between Precipitation, African Easterly Jet, and African East-
720 erly Waves. *Atmosphere*, **11**, 353.

721 Knapp, K.R., M.C. Kruk, D.H. Levinson, H.J. Diamond, and C.J. Neumann, 2010: The Interna-
722 tional Best Track Archive for Climate Stewardship (IBTrACS): Unifying tropical cyclone
723 data. *Bull. Amer. Meteor. Soc.,* **91**, 363–376.

724 Laing A.G., Carbone R., Levizzani V. and J. Tuttle, 2008: The propagation and diurnal cycles
725 of deep convection in northern tropical Africa. *Q. J. Roy. Meteorol. Soc.,* **134**, 93–109.

726 Landsea, C. W., 1993: A climatology of intense (or major) Atlantic hurricanes. *Mon. Wea.*
727 *Rev.*, **121**, 1703–1713.

728 Lavaysse, C., C. Flamant, S. Janicot, and P. Knippertz, 2010: Links between African easterly
729 waves, midlatitude circulation and intraseasonal pulsations of the West African heat low.
730 *Q. J. R. Meteorol. Soc.*, **136**, 141–158.

731 Liebman, B., H. H. Hendon, and J. D. Glick, 1994: The relationship between tropical cy-
732 clones of the western Pacific and Indian Oceans and the Madden–Julian oscillation. *J. Me-*
733 *teor. Soc. Japan,* **72,** 401– 411.

734 Mekonnen, A., C. D. Thorncroft, and A. R. Aiyyer, 2006: Analysis of convection and its as-
735 sociation with African easterly waves. *J. Climate*, **19**, 5405–5421.

736 Mekonnen, A., and W.B. Rossow 2018: The interaction between deep convection and east-
737 erly wave activity over Africa: convective transitions and mechanisms. *Mon. Wea. Rev.*,
738 **146**, 1945– 1961.

739 Menkes, C. E., M. Lengaigne, P. Marchesiello, N. C. Jourdain, E. M. Vincent, J. Lefèvre, F.
740 Chauvin, and J.-F. Royer, 2011: Comparison of tropical cyclogenesis indices on seasonal to
741 interannual timescales, *Climate Dyn.*, **38**, 301– 321.

742 Montgomery, M. T., M. E. Nicholls, T. A. Cram, and A. B. Saunders, 2006: A vortical hot
743 tower route to tropical cyclogenesis. *J. Atmos. Sci.*, **63**, 355–386.

744 Mozer, J. B., and J. A. Zehnder, 1996a: Lee vorticity production by large-scale tropical
745 mountain ranges. Part I: Eastern North Pacific tropical cyclogenesis. *J. Atmos. Sci.*, **53**, 521–
746 538

747 Mozer, J. B., and J. A. Zehnder, 1996b: Lee vorticity production by large-scale tropical
748 mountain ranges. Part II: A Mechanism for the Production of African Waves. *J. Atmos. Sci.*,
749 **53**, 539–549.

750 Nitta, T., and Y. Takayabu, 1985: Global analysis of the lower tropospheric disturbances
751 in the Tropics during the northern summer of the FGGE year. Part II: Regional character-
752 istics of the disturbances. *Pure Appl. Geophys.,* **123,** 272–292.

753 Patricola C.M., R. Saravanan, and P. Chang, 2018: The response of Atlantic tropical cy-
754 clones to suppression of African easterly waves. *Geophys. Res. Lett.*, **45**, 471–479.

755 Pytharoulis, I., and C. Thorncroft, 1999: The low-level structure of African easterly waves
756 in 1995. *Mon. Wea. Rev.*, **127**, 2266–2280.

757 Reed, R. J. , D. C. Norquist, and E. E. Recker, 1977: The structure and properties of African
758 wave disturbances as observed during Phase III of GATE. *Mon. Wea. Rev.,* **105,** 317–333.

759 Reed, R. J., E. Klinker, and A. Hollingsworth, 1988a: The structure and characteristics of
760 African easterly wave disturbances as determined from the ECMWF operational analy-
761 sis/forecast system. *Meteor. Atmos. Phys.*, **38**, 22–33.

762 Reed, R. J., A. Hollingsworth, W. A. Heckley, and F. Delsol, 1988b: An evaluation of the per-
763 formance of the ECMWF operational forecasting system in analyzing and forecasting trop-
764 ical easterly wave disturbances over Africa and the tropical Atlantic. *Mon. Wea. Rev.,* **116,**
765 824–865.

766 Ritchie, E. A., and G. J. Holland, 1997: Scale interactions during the formation of Typhoon
767 Irving. *Mon. Wea. Rev.*, **125**, 1377– 1396.

768 Ross, R. S., and T. N. Krishnamurti, 2007: Low-level African easterly wave activity and its
769 relation to Atlantic tropical cyclogenesis in 2001. *Mon. Wea. Rev.* **135**: 3950 – 3964.

770 Russell, J. O., A. Aiyyer, J. D. White, and W. Hannah, 2017: Revisiting the connection be-
771 tween African Easterly Waves and Atlantic tropical cyclogenesis. *Geophys. Res. Lett.*, **44**,
772 587–595.

773 Thorncroft, C. D., and B. J. Hoskins, 1994: An idealized study of African easterly waves.
774 Part II: A nonlinear view. *Quart. J. Roy. Meteor. Soc.,* **120,** 983–1015.

775 Thorncroft, C. D., and K. Hodges, 2001: African easterly wave variability and its relation-
776 ship to Atlantic tropical cyclone activity. *J. Climate,* **14,** 1166–1179.

777 Tippett, M. K., Camargo, S. J. & Sobel, A. H., 2011: A Poisson regression index for tropical
778 cyclone genesis and the role of large-scale vorticity in genesis. *J. Climate*, **24**, 2335–2357.

779 Wang, Z., M. T. Montgomery, and C. Fritz, 2012: A first look at the structure of the wave
780 pouch during the 2009 PREDICT-GRIP dry runs over the Atlantic. *Mon. Wea. Rev.*, **4**, 1144–
781 1163.

782 Wu, M. C., O. Reale, S. D. Schubert, M. J. Suarez, R. D. Koster, and P. J. Pegion, 2009: African
783 Easterly Jet: Structure and Maintenance, *J. Climate*, **22**, 4459–4480.

784 Zhang, Y. C., F. Q. Zhang, C. A. Davis, and J. H. Sun, 2018: Diurnal evolution and structure of
785 long-lived mesoscale convective vortices along the Mei-yu front over the East China
786 plains. *J. Atmos. Sci.*, **75**, 1005–1025.
787

788

Acronyms Specific terms	Definition
Vortex	A vortex is defined here as a synoptic-scale circulation around a local minimum in the geopotential height of a given pressure level. This is equivalent to a closed circulation, or a minimum of the streamfunction, in the geostrophic approximation. We consider that this approximation is valid in most cases even if it is not strictly the case for some of the smaller vortices. The term vortex also refers to the entire life cycle of a vortex disturbance moving over West Africa and the Atlantic Ocean.
Vortex track	A vortex track is a time series of consecutive barycenter positions of a given moving vortex. We consider only vortex tracks initiated over the domain 60°W-50°E and 0°N-30°N. The tracking is done for a larger domain 130°W-50°E and 0°N-60°N.
Atlantic Vortex (AV)	An AV is a vortex that spend at least one day over the Atlantic Ocean and enters the domain south of 20°N.
North path	The north path is the ensemble of low-level (850 hPa) AV initiated over West Africa north of 15°N and east of 10°W.
South path	The south path is the ensemble of mid-level (700 hPa) AV initiated over West Africa south of 15°N and east of 10°W.
Main Development Region (MDR)	The MDR is the domain extending from 10°W to 60°W and from 5°N to 20°N.
Cyclogenetic Atlantic Vortex (CAV)	A CAV is an AV that has at least one barycenter position within 3° of an IBTrACS system. More than 97% of CAVs have more than 4 consecutive positions (1 day) in common with their IBTrACS system.
Non-Cyclogenetic Atlantic Vortex (NCAV)	An NCAV is an AV with all barycenter positions at more than 3° from any IBTrACS system.
AV Merging	A merging of a low-level (850 hPa) and a mid-level (700 hPa) AV occurs when they are within 3° of each other for the first time. After merging, the two AV tracks are nearly identical in most cases (e.g. figure 1).
Primary AV	When two AVs merge, the primary AV is the older at merging time.
Secondary AV	When two AVs merge, the secondary AV is the younger at merging time.
Confluence	If both AVs are initiated long before merging (e.g. ≥1 day), the merging is called a "confluence" of the two vortex tracks.
Vertical expansion (deepening)	If the secondary AV is initiated shortly before merging (e.g. <1 day), the merging corresponds more to a vertical expansion (or deepening) of the primary AV.

789 Table 1: Definition of different acronyms and specific terms.

790

Region of Initiation	Primary AV Initiations				Impact on Cyclogenesis			
	(a) Number of AV initiations		(b) % of CAV		(c) % cyclogenesis MDR		(d) % cyclogenesis Western Regions	
	850 hPa	*700 hPa*	*850 hPa*	*700 hPa*	*850 hPa*	*700 hPa*	*850 hPa*	*700 hPa*
North Path	**428**	32	**10**	16	**16**	2	**5**	0
South Path	54	**424**	26	**23**	6	**38**	1	**6**
Continent, east of 10°W	482	456	12	23	22	40	6	6
	938		17		62		12	
Atl. and coast, west of 10°W	562	770	11	9	18	20	11	14
	1332		10		38		25	

Table 2 : Statistics on (a) the number of primary AV initiations and (b) the percentage of cyclogenetic AV (CAV) for different regions of initiation and contribution of AVs coming from these initiation regions to cyclogenesis (c) over the MDR and (d) over regions west of 60°W and south of 20°N. North and south path initiation regions are located east of 10°W and north and south of 15°N, respectively (Fig.1). The "continent" statistics corresponds to the summation of north and south path statistics. The statistics are shown for each pressure level (850 hPa and 700 hPa) and on average for both pressure levels for the continent and for the Atlantic and coastal regions. Numbers in bold represent the main contribution for the north and the south path.

803 **Figure captions**

804 Figure 1: Domain of vortex initiations (thin black) and more specifically for the north
805 (blue) and the south (red) path vortices. The limits of the Main Development Region
806 (MDR) (magenta) include longitudes between 10°W and 60°W. Also shown is an example
807 for two vortex tracks, merging near the coast, and at the origin of tropical cyclone Edouard
808 in September 2014 (markers are drawn one day apart). "Atlantic and coast" and
809 "Continent" refer to areas west and east of 10°W, respectivelly.

810 Figure 2: Initiation density of the barycenter of all Atlantic Vortices (AV) detected at (a)
811 700 hPa and (b) 850 hPa between June and October 1980-2017. AV are vortices spending
812 at least one day over the Atlantic Ocean. Fields are smoothed by a 5°x5° running mean.
813 The first contour (dotted line) is 0.5 and the increment is 1. The total number of AV initi-
814 ations is reported in the upper right corners.

815 Figure 3: As in figure 2 but for AV tracks that do not merge with an AV track of the other
816 pressure level.

817 Figure 4: As in figure 2, but for initiation density of the barycenter of Not Cyclogenetic
818 Atlantic Vortices (NCAV) detected at (a) 700 hPa and (b) 850 hPa and that merge with a
819 secondary AV track of the other pressure level. (c) Initiation density of secondary vortices
820 at 850 hPa associated with a primary vortex at 700 hPa. (d) Initiation density of secondary
821 vortices at 700 hPa associated with a primary vortex at 850 hPa. Merging position density
822 for the barycenter of the primary vortices at (e) 700 hPa and (f) 850 hPa. The first contour
823 (dotted line) is 0.5 and the increment is 1.

824 Figure 5: As in figure 4, but for initiation density of Cyclogenetic Atlantic Vortices (CAV).
825 The bottom panel represents the density of the first match between a CAV and an IBTrACS

826 system for (g) 700 hPa and (h) 850 hPa primary vortices. This match generally corre-
827 sponds to the first time-step of an IBTrACS system and is considered here as a cyclogene-
828 sis. The first contour (dotted line) is 0.125 and the increment is 0.25.

829 Figure 6: Track density for AVs that do not merge (a, b), primary merging NCAV (c, d), and
830 corresponding secondary NCAV at the other level (e, f). The first contour (dotted line) is
831 0.5 and the increment is 1.

832 Figure 7: As in figure 6 for primary CAVs (a, b) and corresponding secondary CAVs (c, d).
833 The first contour (dotted line) is 0.125 and the increment is 0.25.

834 Figure 8: Seasonal variation of the average monthly number of primary AV (N_{AV}: filled
835 circles) and CAV (N_{CAV}: open circles) initiations at 700 hPa (red) and 850 hPa (blue) for
836 (a) merging AV initiated near the coast (between 10°W and 20°W); (b) merging AV initi-
837 ated over West Africa (east of 10°W); (c) and (d), as for (a) and (b), but for non-merging
838 AV.

839 Figure 9: Seasonal variations of (a) cyclogenetic efficiency (CE) and (b) merging efficiency
840 (ME) for primary AV initiated east of 10°W and (red) south of 15°N at 700 hPa, (blue)
841 north of 15°N at 850 hPa. (black) average for both paths. (c) as in (a) but for interannual
842 variations of the mean CE for August and September.

843 Figure 10: Longitudinal distribution of the proportion of cyclogenesis as a function of the
844 easternmost initiation region of the CAV at either 700 hPa or 850 hPa: (red) West Africa,
845 (green) Coast and (blue) Ocean. The dotted curve represents the longitudinal distribution
846 of the season-average number of cyclogenesis.

847 Figure 11: Longitudinal distribution of the average vortex intensity (maximum Δgz in the
848 "vortex area") for primary CAV and NCAV tracks initiated east of 10°W and between (a)
849 5°N and 15°N at 700 hPa and (b) 15°N and 25°N at 850 hPa. (c) and (d), as for (a) and (b),

but for the average vortex intensity as a function of the delay relative to the vortex deepening for deepening occurring west of 10°W (i.e. for already formed continental AVs). The shading represents the uncertainty on the average values for a 99% significance level. In (c) and (d), the bar graph represents the number of vortices with a given delay between vortex deepening and cyclogenesis.

Figure 12: Schematic illustrating the four merging categories of the 700 hPa (red) and the 850 hPa (blue) vortex tracks: (a) merging of vortices of the north and the south path, (b) local vortex development, (c) downward expansion of a vortex of the south path and, (d) upward expansion of a vortex of the north path. The proportion of each merging category is reported in the lower left.

Figure 13: Initiation density (#/season/10° box) for (red) 700 hPa and (blue) 850 hPa Atlantic Vortices belonging to the four merging categories a, b, c and d of figure 12. The first contour (dotted line) is 1 and the increment is 1. The black dots correspond to the location of cyclogenesis (first match with an IBTrACS system). The proportion of merge and of cyclogenesis are reported in the upper right boxes for each category. Fields are smoothed by a 5°x5° running mean.

Figure 14: As in figure 13, but for the merging density. The first contour (dotted line) is 1 and the increment is 1.

Figure 15: Seasonal variation of the number of merges due to AV (red) and to CAV (black) for the four merging categories of figure 12. The grey filled curves represent the cyclogenesis efficiency.

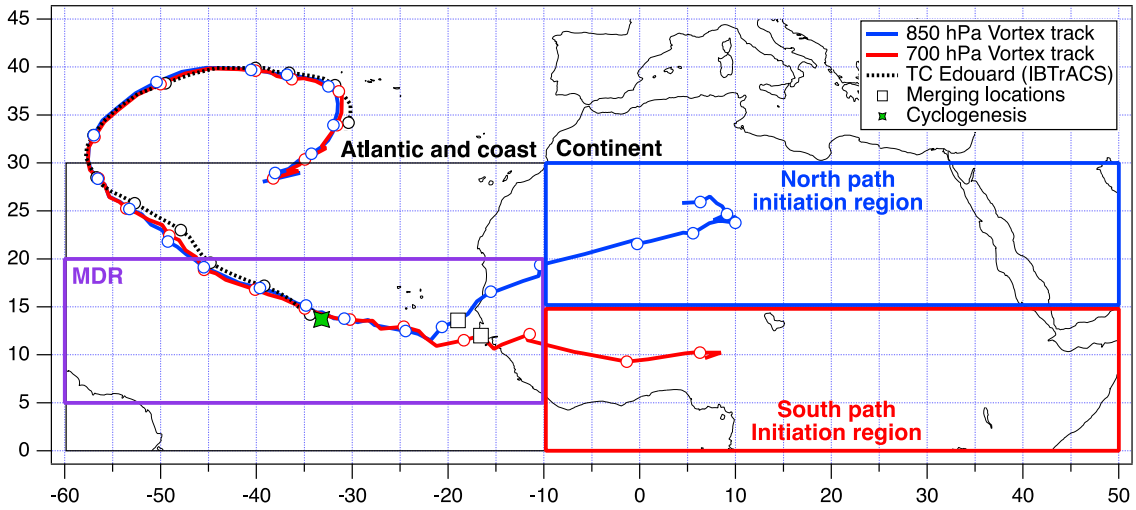

Figure 1: Domain of vortex initiations (thin black) and more specifically for the north (blue) and the south (red) path vortices. The limits of the Main Development Region (MDR) (magenta) include longitudes between 10°W and 60°W. Also shown is an example for two vortex tracks, merging near the coast, and at the origin of tropical cyclone Edouard in September 2014 (markers are drawn for 00GMT). “Atlantic and coast” and “Continent” refer to areas west and east of 10°W, respectivelly.

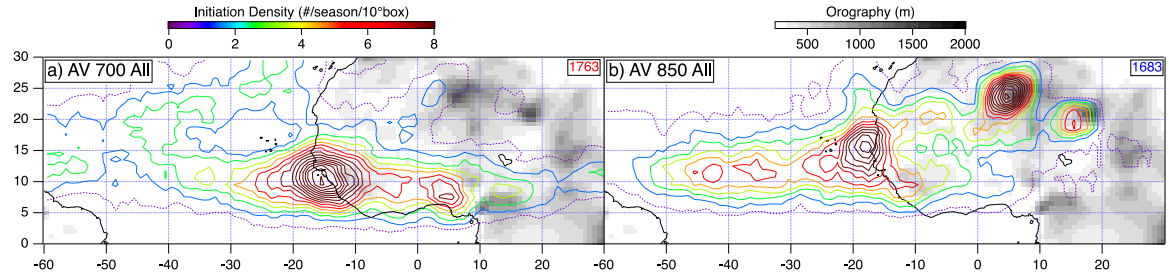

Figure 2: Initiation density of the barycenter of all Atlantic Vortices (AV) detected at (a) 700 hPa and (b) 850 hPa between June and October 1980-2017. AV are vortices spending at least one day over the Atlantic Ocean. Fields are smoothed by a 5°x5° running mean. The first contour (dotted line) is 0.5 and the increment is 1. The total number of AV initiations is reported in the upper right corners.

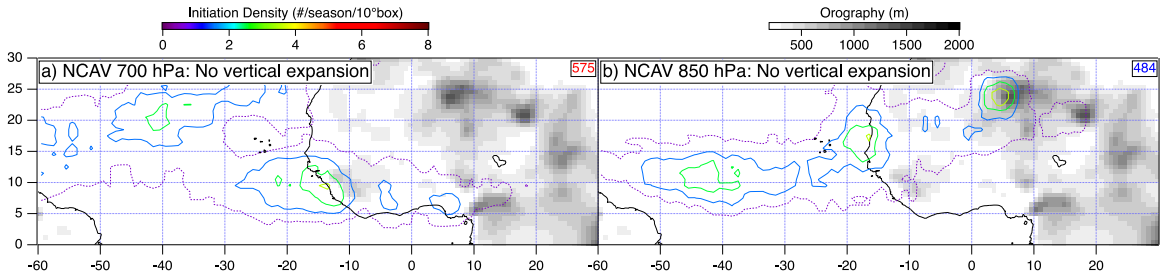

Figure 3: As in figure 2 but for AV tracks that do not merge with an AV track of the other pressure level.

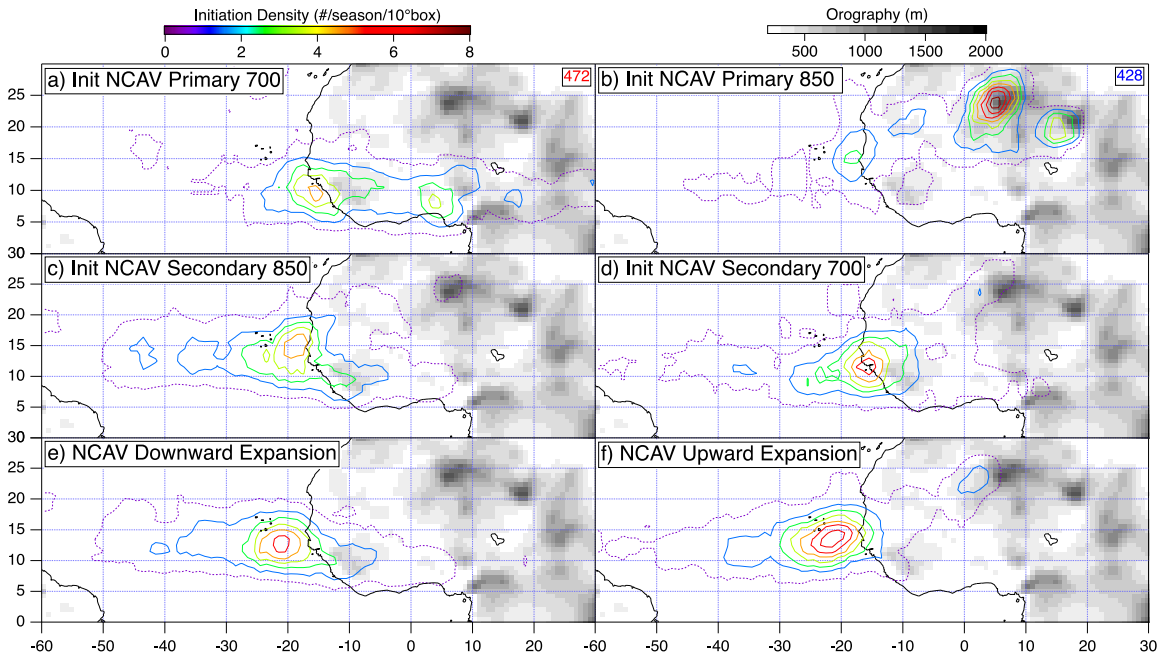

Figure 4: As in figure 2, but for initiation density of the barycenter of Not Cyclogenetic Atlantic Vortices (NCAV) detected at (a) 700 hPa and (b) 850 hPa and that merge with a secondary AV track of the other pressure level. (c) Initiation density of secondary vortices at 850 hPa associated with a primary vortex at 700 hPa. (d) Initiation density of secondary vortices at 700 hPa associated with a primary vortex at 850 hPa. Merging position density for the barycenter of the primary vortices at (e) 700 hPa and (f) 850 hPa. The first contour (dotted line) is 0.5 and the increment is 1.

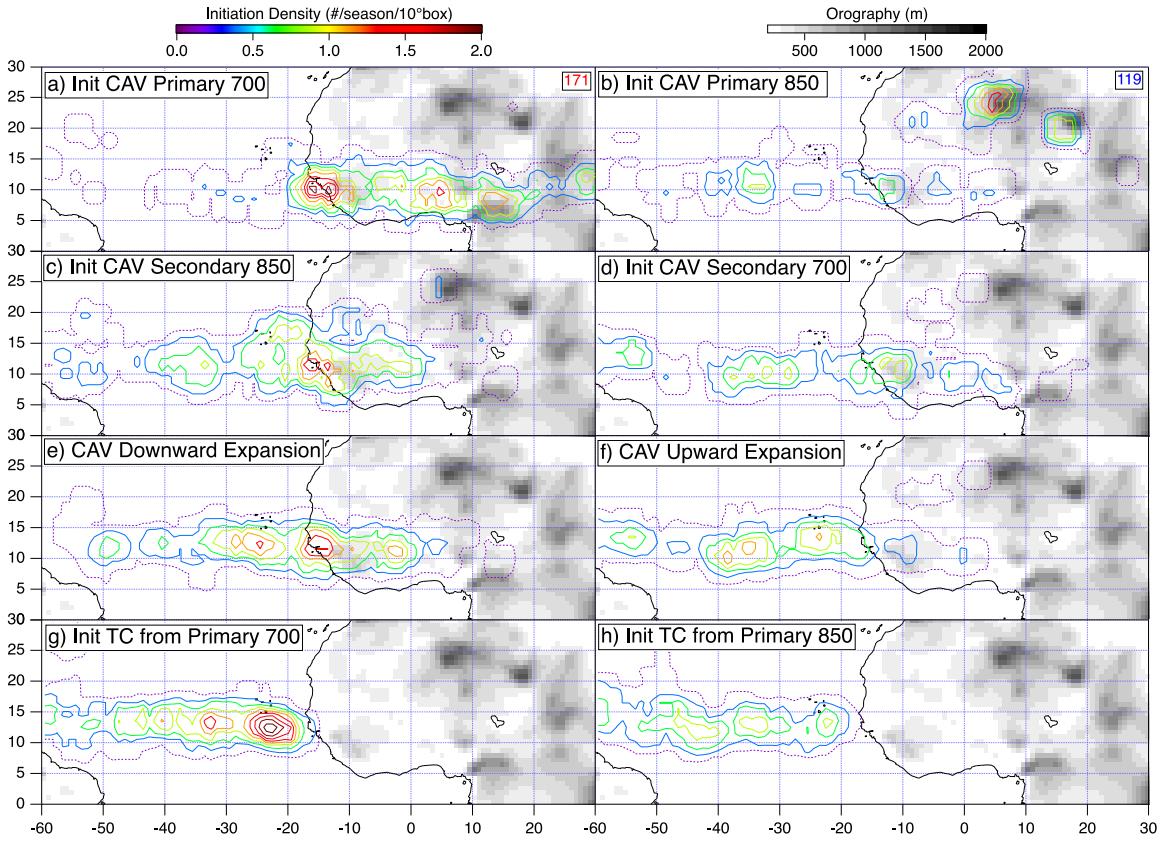

Figure 5: As in figure 4, but for initiation density of Cyclogenetic Atlantic Vortices (CAV). The bottom panel represents the density of the first match between a CAV and an IBTrACS system for (g) 700 hPa and (h) 850 hPa primary vortices. This match generally corresponds to the first time-step of an IBTrACS system and is considered here as a cyclogenesis. The first contour (dotted line) is 0.125 and the increment is 0.25.

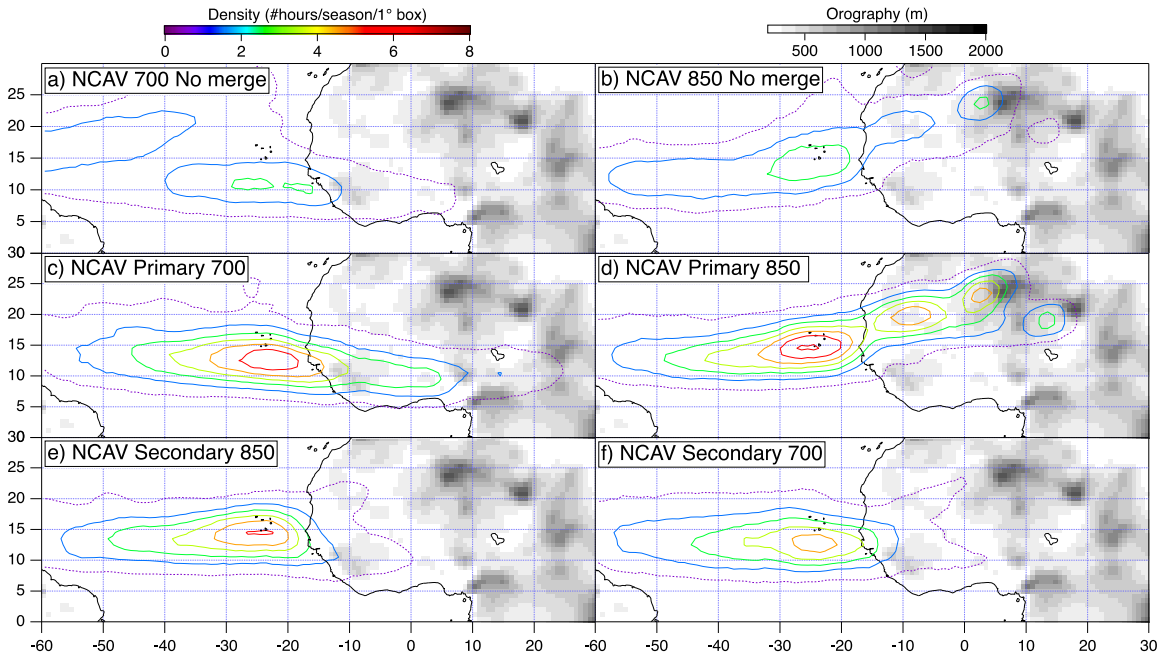

Figure 6: Track density for AVs that do not merge (a, b), primary merging NCAV (c, d), and corresponding secondary NCAV at the other level (e, f). The first contour (dotted line) is 0.5 and the increment is 1.

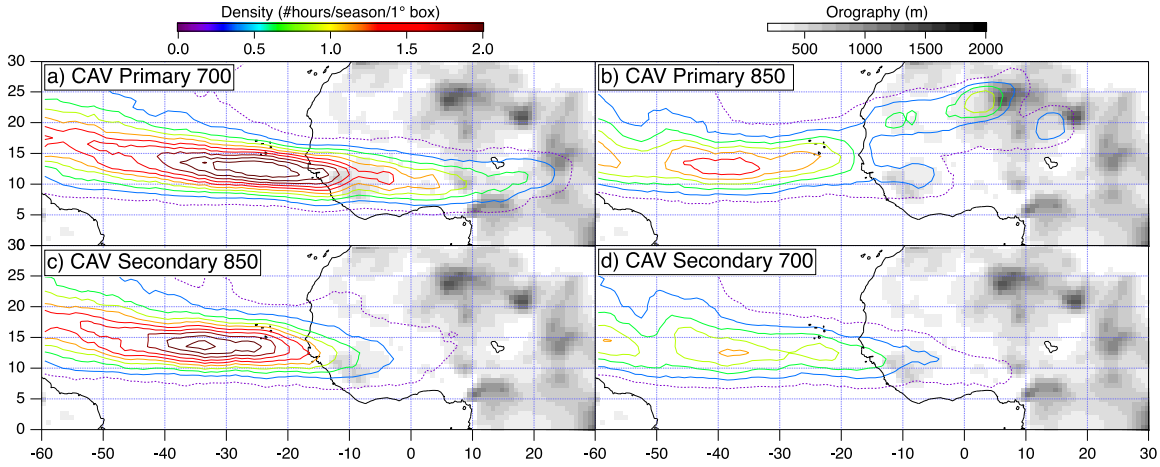

Figure 7: As in figure 6 for primary CAVs (a, b) and corresponding secondary CAVs (c, d).

The first contour (dotted line) is 0.125 and the increment is 0.25.

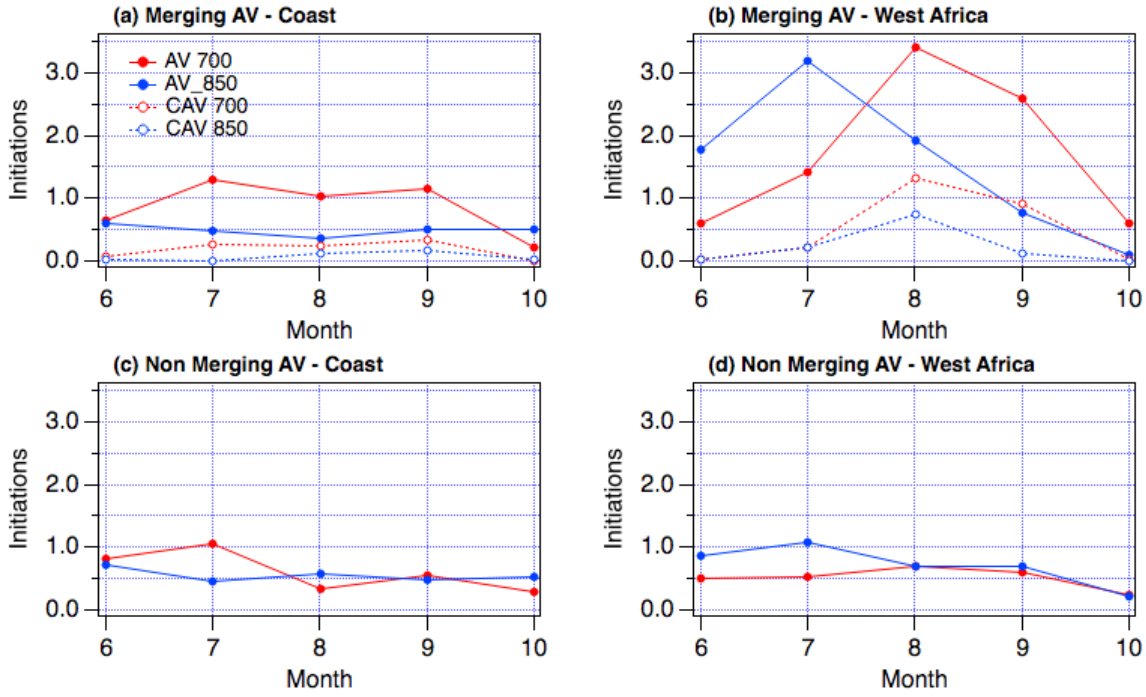

Figure 8: Seasonal variation of the average monthly number of primary AV (N_{AV}: filled circles) and CAV (N_{CAV}: open circles) initiations at 700 hPa (red) and 850 hPa (blue) for (a) merging AV initiated near the coast (between 10°W and 20°W); (b) merging AV initiated over West Africa (east of 10°W); (c) and (d), as for (a) and (b), but for non-merging AV.

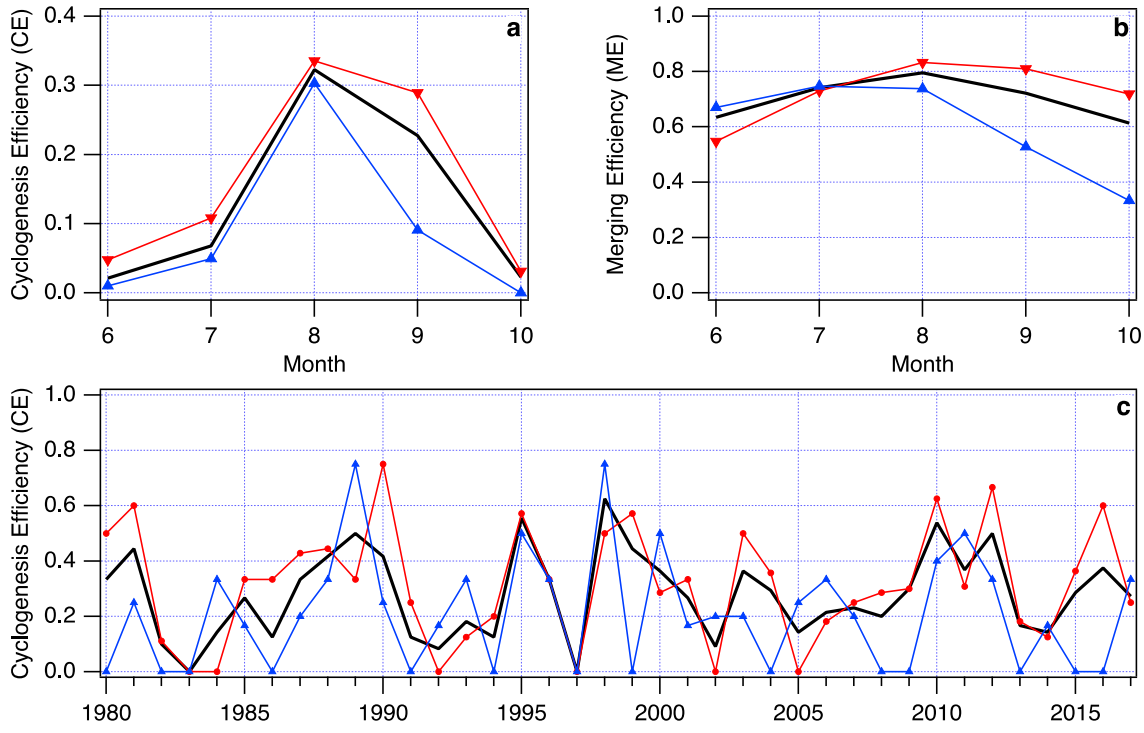

Figure 9: Seasonal variations of (a) cyclogenetic efficiency (CE) and (b) merging efficiency (ME) for primary AV initiated east of 10°W and (red) south of 15°N at 700 hPa, (blue) north of 15°N at 850 hPa. (black) average for both paths. (c) as in (a) but for interannual variations of the mean CE for August and September.

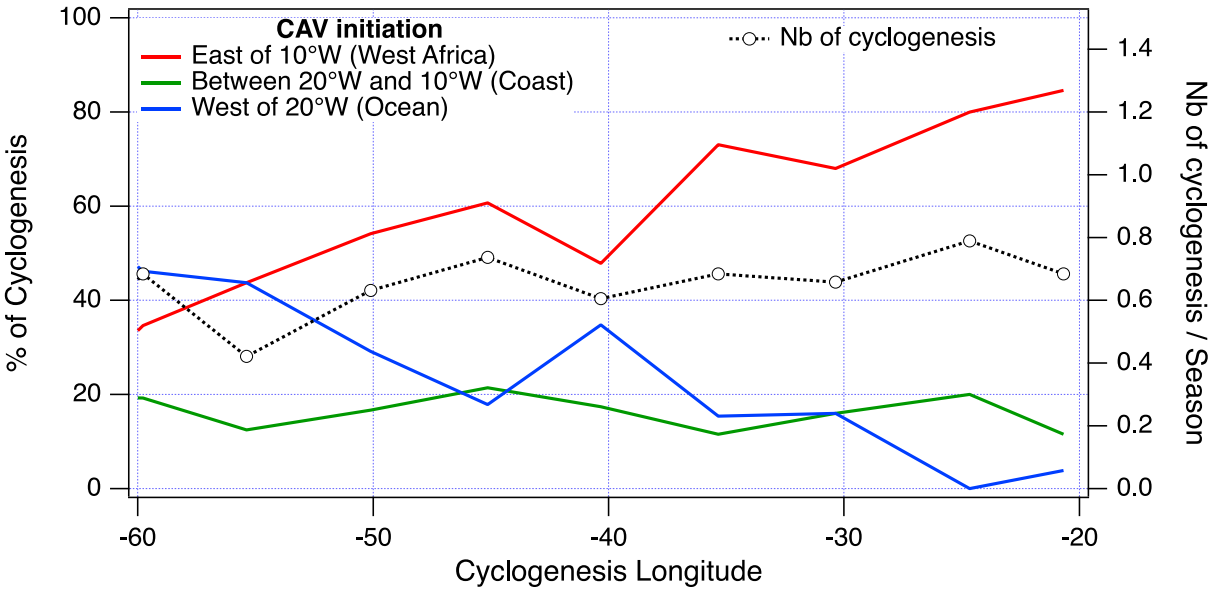

Figure 10: Longitudinal distribution of the proportion of cyclogenesis as a function of the easternmost initiation region of the CAV at either 700 hPa or 850 hPa: (red) West Africa, (green) Coast and (blue) Ocean. The dotted curve represents the longitudinal distribution of the season-average number of cyclogenesis.

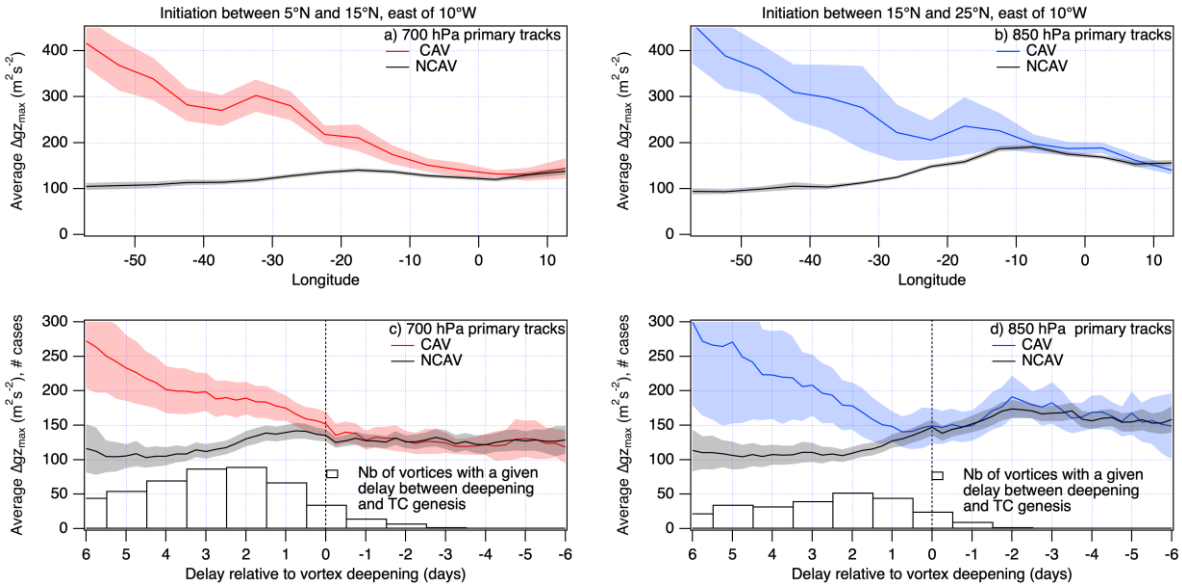

Figure 11: Longitudinal distribution of the average vortex intensity (maximum Δgz in the "vortex area") for primary CAV and NCAV tracks initiated east of 10°W and between (a) 5°N and 15°N at 700 hPa and (b) 15°N and 25°N at 850 hPa. (c) and (d), as for (a) and (b), but for the average vortex intensity as a function of the delay relative to the vortex deepening for deepening occurring west of 10°W (i.e. for already formed continental AVs). The shading represents the uncertainty on the average values for a 99% significance level. In (c) and (d), the bar graph represents the number of vortices with a given delay between vortex deepening and cyclogenesis.

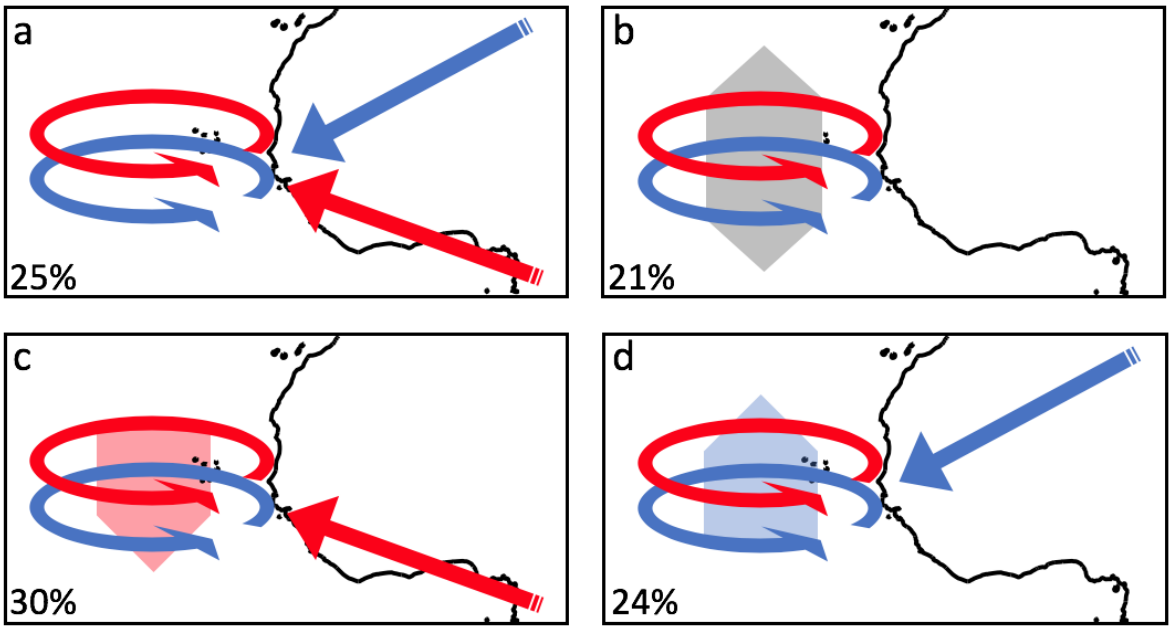

Figure 12: Schematic illustrating the four merging categories of the 700 hPa (red) and the 850 hPa (blue) vortex tracks: (a) merging of vortices of the north and the south path, (b) local vortex development, (c) downward expansion of a vortex of the south path and, (d) upward expansion of a vortex of the north path. The proportion of each merging category is reported in the lower left.

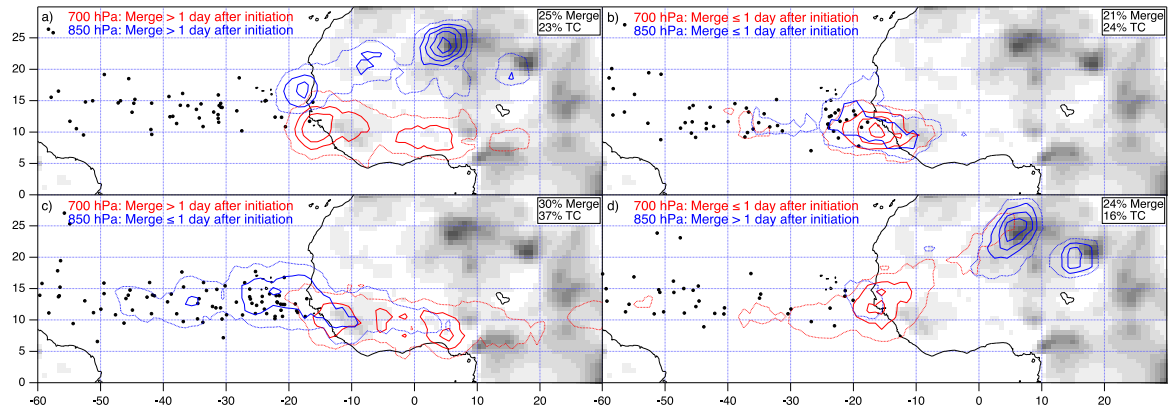

Figure 13: Initiation density (#/season/10° box) for (red) 700 hPa and (blue) 850 hPa Atlantic Vortices belonging to the four merging categories a, b, c and d of figure 12. The first contour (dotted line) is 1 and the increment is 1. The black dots correspond to the location of cyclogenesis (first match with an IBTrACS system). The proportion of merge and of cyclogenesis are reported in the upper right boxes for each category. Fields are smoothed by a 5°x5° running mean.

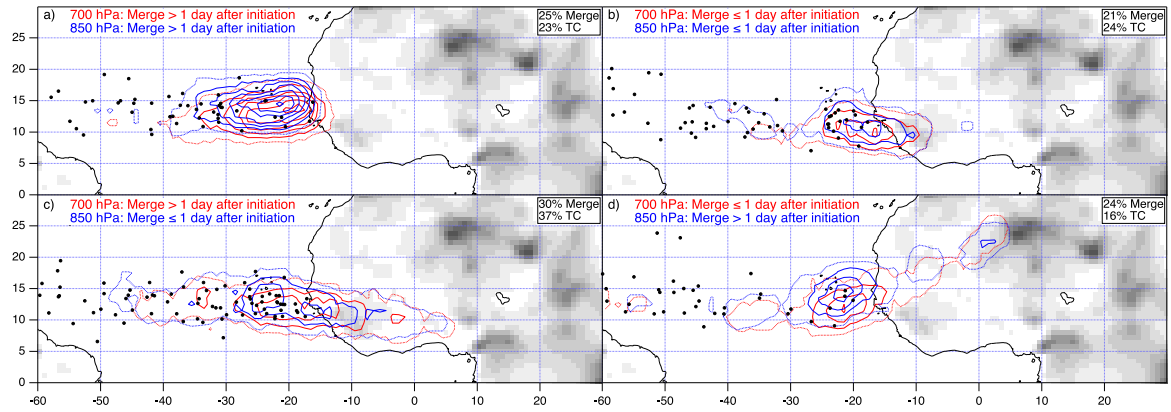

Figure 14: As in figure 13, but for the merging density. The first contour (dotted line) is 1 and the increment is 1.

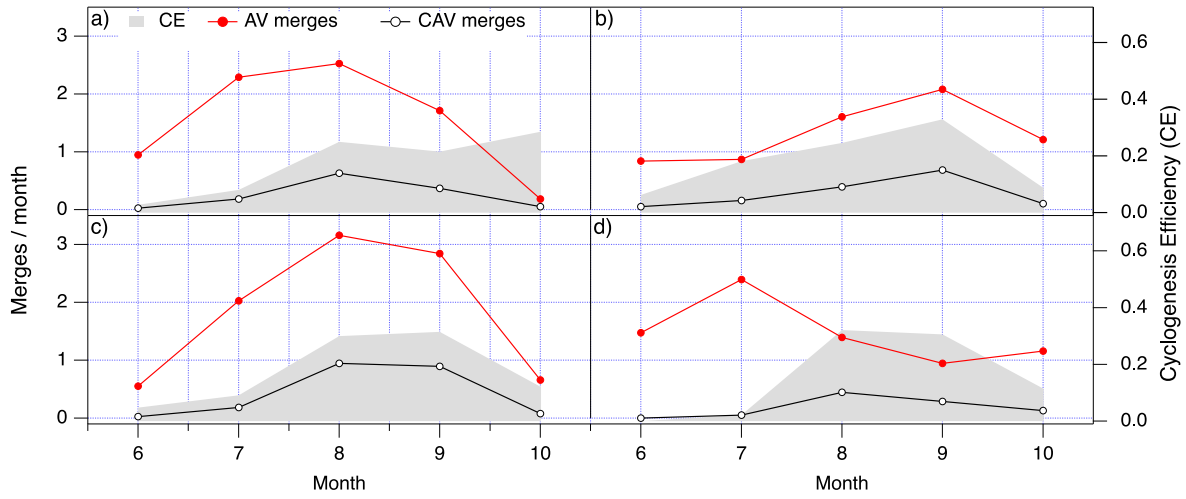

Figure 15: Seasonal variation of the number of merges due to AV (red) and to CAV (black) for the four merging categories of figure 12. The grey filled curves represent the cyclogenesis efficiency.